Vol. 25, No. 3(2026) Mat26864
Materiales
Revista Mexicana de Ingeniería Química

Influence of niobium on the microstructure, hardness, wear and impact resistance of austempered ductile iron

Influencia del niobio en la microestructura, la dureza, el desgaste y la resistencia al impacto del hierro nodular austemperizado

C.Y. Becerra-Mayorga[1]*, M. Vargas-Ramírez[1], E. Cardoso-Legorreta[1], F. Hernández-Santiago[2]

[1]Instituto de Ciencias Básicas e Ingeniería, Universidad Autónoma del Estado de Hidalgo, Carretera Pachuca-Tulancingo Km. 4.5, Colonia Carboneras, Mineral de la Reforma, Hidalgo, México, C.P. 42184.
[2]ESIME - Escuela Superior de Ingeniería Mecánica y Eléctrica Unidad Azcapotzalco Instituto Politécnico Nacional, Av. de las Granjas 682, Santa Catarina, Azcapotzalco, Ciudad de México, México, C.P. 02550.
Received: May 4, 2026; Accepted: July 9, 2026

Abstract

This study investigates the effect of niobium additions on the microstructure, wear resistance, hardness, and impact toughness of austempered ductile iron (ADI). Austempering treatments were performed at 250 °C and 300 °C for 15, 30, 60, and 90 min. The highest retained high-carbon austenite fraction (42.79%) was obtained in the alloy containing 0.3 wt.% Nb austempered at 250 °C for 60 min. The maximum hardness value (40.36 HRC) was achieved in the 0.3 wt.% Nb alloy austempered at 250 °C for 15 min. Regarding wear behavior, the lowest volume loss (1.35 mm^3) was recorded for the 0.3 wt.% Nb alloy austempered at 250 °C for 15 min, indicating superior wear resistance under these conditions. The results show that niobium additions influence the microstructural evolution and mechanical performance of ADI, promoting higher retained austenite fractions and improved wear resistance under selected austempering conditions.
Keywords: Austempered, High carbon austenite, austempered ductile iron, niobium.

Resumen

Este estudio investiga el efecto de la adición de niobio sobre la microestructura, la resistencia al desgaste, la dureza y la tenacidad al impacto del hierro nodular austemperizado (ADI). Los tratamientos de austemperizado se realizaron a 250 °C y 300 °C durante 15, 30, 60 y 90 min. La mayor fracción de austenita retenida de alto contenido de carbono (42.79 %) se obtuvo en la aleación con 0.3 % en peso de Nb austemperizada a 250 °C durante 60 min. El valor máximo de dureza (40.36 HRC) se alcanzó en la aleación con 0.3 % en peso de Nb austemperizada a 250 °C durante 15 min. En cuanto al comportamiento al desgaste, la menor pérdida de volumen (1.35 mm^3) se registró en la aleación con 0.3 % en peso de Nb austemperizada a 250 °C durante 15 min, lo que indica una mayor resistencia al desgaste bajo estas condiciones. Los resultados muestran que las adiciones de niobio influyen en la evolución microestructural y en el desempeño mecánico del ADI, favoreciendo mayores fracciones de austenita retenida y una mejora en la resistencia al desgaste bajo condiciones específicas de austemperizado. Estos hallazgos demuestran el potencial de la adición de niobio, combinada con parámetros de austemperizado adecuados, para optimizar el equilibrio entre el contenido de austenita retenida, la dureza y la resistencia al desgaste en hierros nodulares austemperizados.
Palabras clave: Austemperizado, Austenita con alto contenido de carbono, hierro dúctil, niobio.

*Corresponding author. E-mail: cesar_becerra@uaeh.edu.mx ;
https://doi.org/10.24275/rmiq/Mat26864
ISSN:1665-2738, *issn-e*: 2395-8472

1 Introduction

Nodular graphite iron, commonly known as ductile iron, belongs to the cast iron family and is characterized by its superior ductility, which is primarily attributed to the presence of spheroidal graphite nodules (Artola *et al.*, 2017; Nan *et al.*, 2020; Zhang *et al.*, 2014; Zimba et al., 2003). The mechanical properties of ductile iron can be significantly enhanced through austempering heat treatment, producing a material known as an austempered ductile iron (ADI) (Avdusinovic & Gigović, 2009; Nofal & Jekova, 1982). ADI is an advanced form of ductile iron obtained through a controlled thermal process that results in the formation of a distinctive microstructure called ausferrite, composed of acicular ferrite and high carbon austenite (Janowak *et al.*, 1982; Rouns *et al.*, 1984; Dubensky *et al.*, 1985; Janowak *et al.*, 1985; Górny *et al.*, 2021). The austempering process occurs in two stages. During the first stage, unstable austenite (γ) transforms into acicular ferrite (α_{Acicular}) and high carbon austenite (γ_{HC}), as represented by Eq. (1) (Swain *et al.*, 2012).

$$y \rightarrow a_{Acicular} + y_{HC} \tag{1}$$

If the austempering time increases, the second reaction may occur, in which the high carbon austenite transforms into bainitic ferrite (α_{Bainitic}) and carbides of the ε or Fe_3C type, as shown in Eq. (2). This stage is undesirable as it negatively impacts mechanical properties, promoting brittleness (Pereloma & Anderson, 2013):

$$y_{HC} \rightarrow a_{Bainitic} + Carbides \tag{2}$$

The optimal mechanical performance of ADI is achieved at the conclusion of the first stage and before the onset of the second stage, this interval is known as the "processing window" (Bayati & Elliot, 1999). During this period, ferrite and high carbon austenite phases are formed as carbon diffusion from graphite nodules takes place (Zhu *et al.*, 2013).

The quantity and morphology of high carbon austenite and acicular ferrite are highly dependent on austempering parameters such as temperature and holding time (Erfanian *et al.*, 2012). Higher austempering temperatures (e.g., 350 °C) tend to produce coarse ausferrite with larger amounts of high carbon austenite, improving ductility but reducing tensile strength. In contrast, lower austempering temperatures (e.g., 250 °C) result in fine ausferrite with reduced high carbon austenite, leading to higher tensile strength at the expense of ductility (Darwish & Elliot, 2013; Boccardo *et al.*, 2018; Górny *et al.*, 2019). In recent years, increasing attention has been directed toward optimizing the properties of ADI through microalloying with elements such as copper, molybdenum, vanadium and particularly niobium. Although niobium has shown potential for refining microstructures and improving mechanical performance, its role in ADI remains insufficiently explored and somewhat controversial, especially in relation to its influence on phase transformations, carbide precipitation and toughness. The role of niobium (Nb) as an alloying element in ductile iron is a relatively recent area of study compared to more traditional additions. Wang *et al.* (2024) reported that niobium addition degrades graphite morphology and promotes pearlite formation. Their mechanical analysis showed that adding Nb to ductile iron increases hardness and strength but reduces elongation and impact resistance. Additionally, Nb has been found to promote carbide formation, which enhances wear and corrosion resistance (Sckudlarek *et al.*, 2021; Chen *et al.*, 2024). Some studies indicate that controlled Nb additions can refine austenite grain size during the austenitization stage (Ahmed *et al.*, 2021). In ADI, the presence of niobium above 0.2 % has been shown to enhance strength and ductility through the formation of a fine ausferritic matrix dispersed NbC nanoprecipitates (Abdullah *et al.*, 2012). The combined effect of niobium content and austempering conditions on transformation kinetics, ausferrite morphology and mechanical properties is not yet fully understood. In particular, the trade-off between increased hardness and reduced impact toughness requires a more systematic assessment. Furthermore, limited research has addressed how niobium affects the stability of high carbon austenite and the evolution of mechanical behavior during austempering at different temperatures. This gap in understanding is critical for application that demands an optical balance between wear resistance and toughness.

Several studies have been carried out to investigate the tribological behavior of ADIs. These studies have shown that wear resistance is influenced by the presence of graphite nodules in the matrix, as well as the amount of high carbon austenite (Chiniforush *et al.*, 2016). Straffelini *et al.* (2011) examined the behavior of an ADI under dry rolling-sliding test and found that it exhibited a lower coefficient of friction compared to nitride steel. Lu *et al.* (1990) reported that Cu-Mo alloyed ADIs showed better wear resistance than conventional ductile iron. Mussa *et al.* (2022) studied two ADI grades and found that the sample with a higher content of high carbon austenite (30 %) displayed a higher coefficient of friction under a 300 N load.

The amount of high carbon austenite plays a crucial role in determining the mechanical properties of ADIs, underscoring the importance of its quantification via X-ray diffraction analysis. Wen *et al*. (2019) examined two ADIs containing 1.7 % Ni, austempered at 280 and 380 °C for 2 hours. The sample treated at 380 °C exhibited a higher volume fraction of high carbon austenite, reaching 26.2 %. Similarly, Wang et al. (2017) alloyed an ADI with 0.6 % Cr and austempered it at 270 °C for 90 minutes, obtaining 11.5 % high carbon austenite. Tyrala *et al*. (2019) investigated a Cu-Mo alloyed ADI (0.98 % Cu and 0.15 % Mo) austempered at 380 °C for duration ranging from 2 to 300 minutes. The maximum austenite content was observed at 60 minutes, reaching 32 %.

The objective of this study is to evaluate the effect of different niobium concentrations on key mechanical properties including hardness, impact resistance and wear behavior. Furthermore, this study aims to characterize the influence of niobium on the austempering process, with a particular focus on the formation and distribution of acicular ferrite and high carbon austenite, as observed through X-ray diffraction, optical microscopy and Scanning Electron Microscope. Therefore, this study aims to clarify the microstructural mechanisms associated with niobium additions under two austempering regimes. By doing so, it seeks to provide practical insights into the development of high-performance ADI components suitable for demanding industrial applications.

2 Materials and methods

The production of niobium-alloyed ductile irons was carried out by melting 1018 steel, ferrosilicon and graphite, with niobium introduced via ferroniobium. During pouring, the melt was inoculated with ferrosilicon and nodularized using ferromagnesium. After complete solidification, the casting was sectioned and subjected to austempering heat treatment. This process involved austenitizing at 900 °C for 1 hour, followed by immediate quenching in a salt bath furnace at two different temperatures of 250 and 300 °C for 15, 30, 60 and 90 minutes. Finally, the samples were cooled to room temperature.

Once the heat treatment cycle was completed, metallographic preparation was performed using silicon carbide (SiC) abrasive papers with grit sizes ranging from 50 to 2000, followed by polishing with 1 μm diamond paste. This procedure was essential to properly reveal the graphite nodules under optical microscopy and scanning electron microscopy (SEM). After polishing, a 3% nital solution was used to reveal the ausferritic matrix. In addition, a 10% ammonium persulfate solution heated to 70 °C was employed to selectively reveal and characterize the carbide phase present in the microstructure. X-ray diffraction analysis was carried out using Co- kα_1 radiation. This analysis enabled the calculation of austenite with high carbon content using Eq. (3) (ASTM International, 2025a), Where V_c represents the volume fraction of secondary phases, including graphite and carbides. The terms I_α and I_γ correspond to the diffraction intensities associated with the α (ferrite) and γ (austenite) phases, respectively. The parameters R_α and R_γ are calculated using Eq. (4), in which v denotes the unit cell volume, F is the structure factor multiplied by its complex conjugate, p is the multiplicity factor of the (hkl) reflection, θ is the Bragg diffraction angle, and e^{-2M} represents the Debye–Waller factor, also known as the temperature factor.

$$Vy = \frac{1 - Vc}{1 + \left(\frac{\Sigma I\alpha}{\Sigma Iy}\right)\left(\frac{\Sigma Ry}{\Sigma R\alpha}\right)} \tag{3}$$

$$R = \left(\frac{1}{v^2}\right)\left[|F|^2 p(1+\cos^2 2\theta)/(\sin^2\theta\cos\theta)\right]e^{-2M} \tag{4}$$

Hardness measurements were performed using the Rockwell C scale with a diamond indenter under load of 150 kgf load. Ten measurements were taken per sample, and the reported values represent the arithmetic mean. Wear resistance was evaluated through a pin-on-ring test at a rotational speed of 300 rpm under a load of 45 N for a total of 4000 revolutions. Three measurements were taken per sample, and the results were averaged. The lost volume was calculated according to Eq. (5), as specified in ASTM G132-96 (ASTM International, 2025b).

$$lost\ volume = \frac{D^2 t}{8}\left[2\sin^{-1}\frac{b}{D} - \sin\left(2\sin^{-1}\frac{b}{D}\right)\right] \tag{5}$$

Where D is the ring diameter (mm), t is the specimen width (mm), and b is the average width of the wear scar (mm). Finally, the Charpy impact tests were conducted using a standard Charpy impact machine. The specimens were prepared according to ASTM E23 and the average of three tests was reported for each condition.

To complete the tensile testing, experiments were carried out using an Instron Series 3400 universal testing machine, following the ASTM E8/E8M standard. The elongation, ultimate tensile strength, and yield strength results correspond to the average of four tests per alloy.

3 Results and discussion

3.1 *Chemical analysis*

The chemical composition of both ductile iron alloys was analyzed using a Shimadzu Spark spectrometer. Five measurements were taken along each sample, and the average values are summarized in table 1.

Table 1. Chemical analysis of ductile irons.

Alloy	Chemical composition (%)						
	Carbon	Silicon	Manganese	Sulfur	Phosphorus	Niobium	CE
Ductile iron 0.2%	3.71	2.51	0.37	0.02	0.006	0.23	4.548
Ductile iron 0.3%	3.67	2.61	0.32	0.019	0.009	0.32	4.543

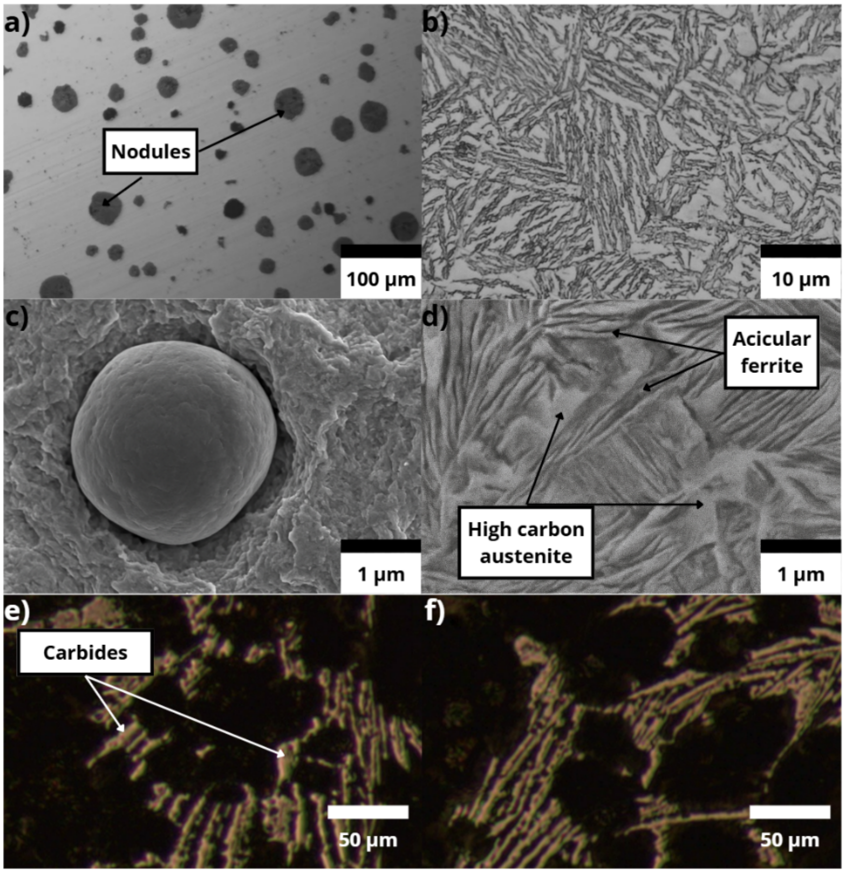

Figure 1. Microstructure of austempered ductile iron with 0.3 % Nb, 30 minutes at 300 °C; a) Nodules observed by optical microscopy; b) ADI observed by optical microscopy; c) Nodule observed by SEM; d) ADI observed by SEM; e) Carbides in 0.2 wt.% Nb ADI and f) Carbides in 0.3 wt.% Nb ADI.

According to Chen *et al*. (2019), the addition of 0.2-0.5 % niobium to ductile iron refines the morphology of the ausferritic structure. Walton (2018) proposed a method for calculating the carbon equivalent (CE), using Eq. (6), which considers carbon, silicon and phosphorus as the main contributing elements. The CE values confirm that both materials correspond to hypereutectic ductile irons.

$$CE = \%C + 1/3(\%Si + \%P) \tag{6}$$

3.2 *Microstructure*

The microstructure obtained after austempering mainly consists of graphite nodules and high carbon austenite (white regions), which result in increased ductility and toughness but reduced hardness and wear resistance. In contrast, the presence of acicular ferrite (dark regiones) enhances hardness and wear resistance while decreasing ductility. A representative microstructure is shown on figure 1. Acicular ferrite forms form unstable austenite through solid-state nucleation and grain growth. At lower austempering temperatures (e.g., 250 °C), faster cooling promotes acicular ferrite formation. Conversely, at higher temperatures (e.g., 300 °C) the microstructure shifts toward coarse ausferrite with a larger volume of high carbon austenite due to slower nucleation rates (Wang *et al*., 2020).

The addition of niobium promotes the formation of NbC carbides due to its strong affinity for carbon. The carbide fraction increased from 1.51% in the 0.2 wt.% Nb alloy to 2.48% in the 0.3 wt.%

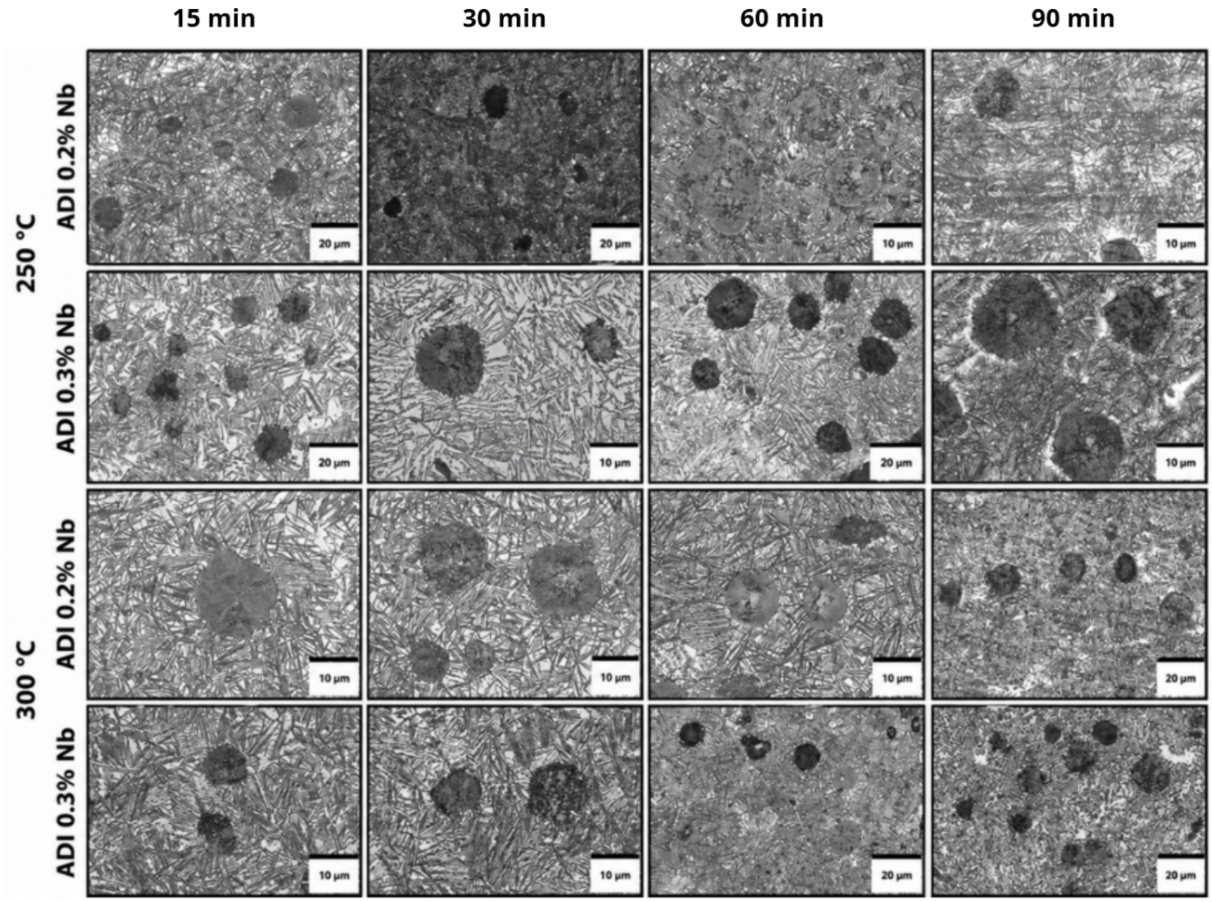

Figure 2. Optical micrographs of 0.2 and 0.3 wt.% Nb ADI austempered at 250 °C and 300 °C for 15, 30, 60, and 90 min.

Nb alloy, confirming that higher niobium additions favor NbC precipitation. These carbides contribute to microstructural refinement and may influence the stabilization of retained high-carbon austenite during austempering. Consequently, the 0.3 wt.% Nb alloy exhibited both a higher carbide fraction and a greater retained austenite content, which may be associated with its improved hardness and wear resistance.

Figure 2 shows the optical microstructures of ADI alloys containing 0.2 and 0.3 wt.% Nb austempered at 250 °C and 300 °C for 15, 30, 60, and 90 min. In all conditions, the microstructure consists of graphite nodules embedded in an ausferritic matrix composed of acicular ferrite and high-carbon retained austenite. Samples austempered at 250 °C exhibit a fine ausferritic structure characterized by thin ferrite plates and a high density of ferrite/austenite interfaces. This refined microstructure is associated with higher hardness, strength, and wear resistance. In contrast, samples austempered at 300 °C show a coarser ausferritic morphology with thicker ferrite plates and a greater amount of retained austenite, resulting from enhanced carbon diffusion at the higher transformation temperature. The alloy containing 0.3 wt.% Nb exhibits a more refined microstructure than the 0.2 wt.% Nb alloy, which may be associated with the presence of NbC particles that contribute to microstructural refinement. Overall, austempering at 250 °C promotes fine ausferrite and improved hardness and wear resistance, whereas austempering at 300 °C favors coarse ausferrite and higher retained austenite contents, enhancing toughness and ductility.

The evolution of the high-carbon retained austenite volume fraction as a function of austempering time is summarized in Table 2, based on the X-ray diffraction results presented in Figure 3. According to equation (3), the highest volume fraction of austenite at 250 °C occurs at 60 minutes, with 41.1 % for ADI 0.2 and 42.79 % for ADI 0.3. At 90 minutes, these values decrease to 38.38 % and 38.07 % respectively, due to the onset of the second austempering reaction, in which high carbon austenite decomposes into ε-type carbides or bainitic ferrite. At 300 °C, the highest austenite content is observed at 30 minutes, with 41.44 % for ADI 0.2 and 42.48 % for ADI 0.3. These values drop to 40.69 % and 40.99 % at 60 minutes, respectively. Higher austempering temperatures accelerate transformation kinetics, narrowing the processing window and leading to faster onset of the second reaction.

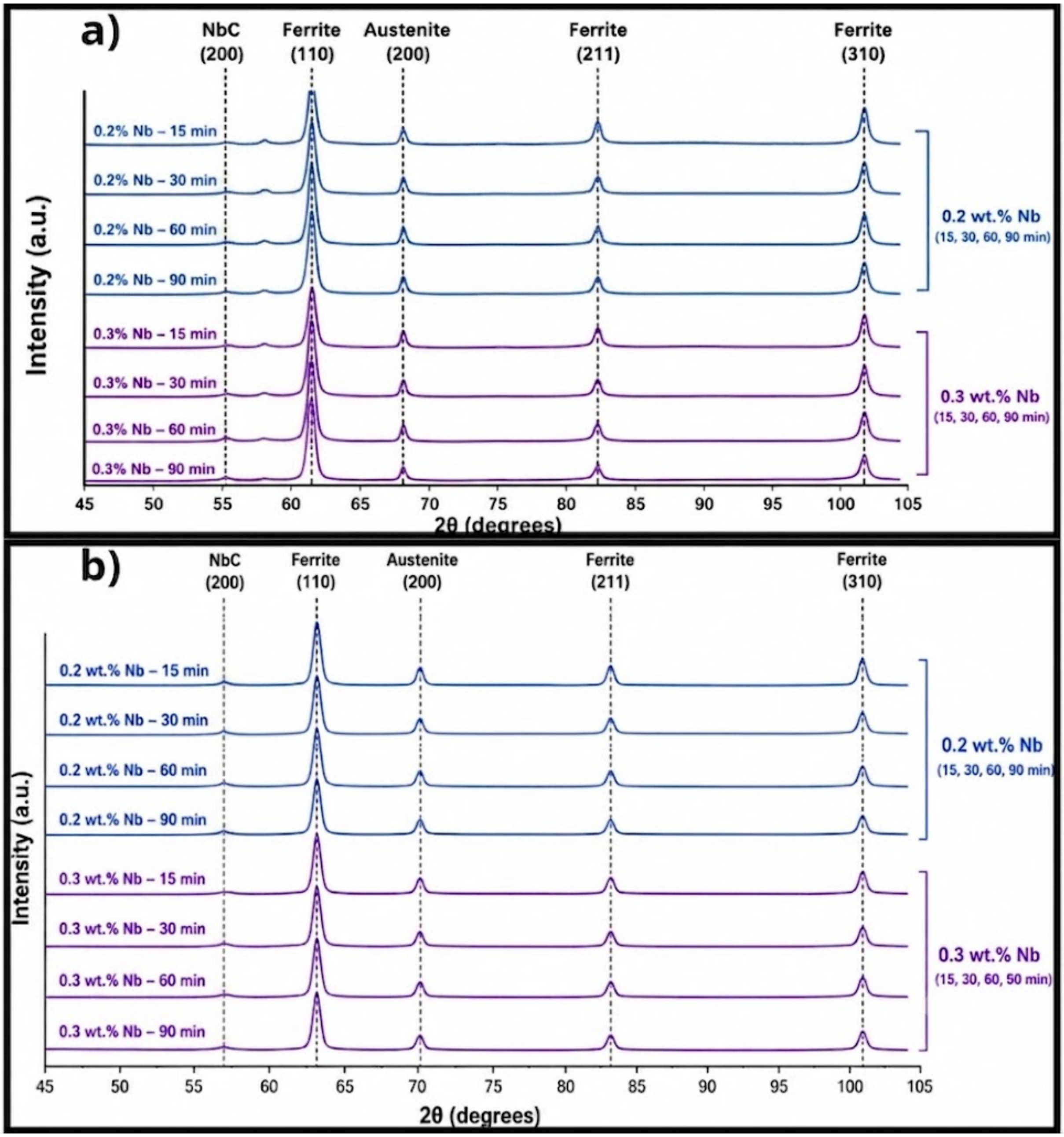

Figure 3. X-ray diffraction patterns of austempered ductile irons containing 0.2 and 0.3 wt.% Nb austempered for 15, 30, 60 and 90 min at: (a) 250 °C and (b) 300 °C. The diffraction peaks corresponding to ferrite, high-carbon austenite and NbC are indicated.

3.3 Tensile test

Figure 4 shows the stress-strain curves of austempered ductile iron samples treated at 250 °C with four different niobium compositions (from 0.2 to 0.3 wt% Nb). The results indicate that the mechanical strength is governed by the refinement of the ausferritic microstructure and precipitation strengthening induced by niobium. Increasing the austempering time promotes microstructural stabilization and enhances strength, while Nb addition intensifies these effects by increasing the density of nucleation sites and promoting the formation of NbC precipitates. As a result, a systematic shift of the curves toward higher stress levels is observed, accompanied by a slight reduction in ductility. This behavior confirms that treatment at 250 °C is optimal for maximizing the mechanical strength of ADI, particularly in alloys with higher Nb content.

The stress-strain curves of ADI austempered at 300 °C, shown in figure 5, reveal a mechanical behavior dominated by the stability of retained austenite and the development of a coarser ausferritic microstructure, resulting in reduced mechanical

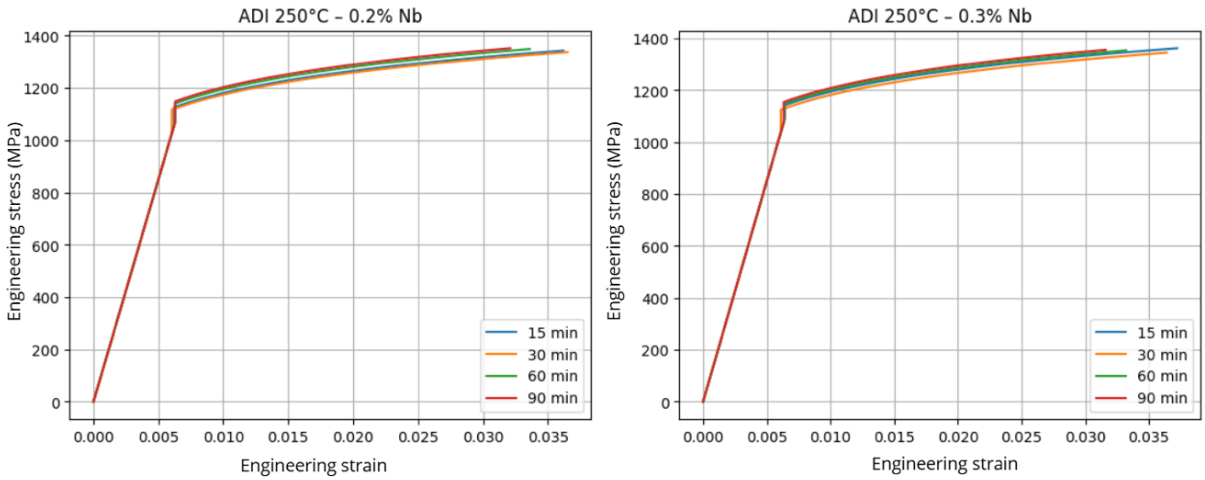

Figure 4. Engineering stress–strain curves of austempered ductile iron at 250 °C for different Nb contents (0.2 and 0.3 wt.%) and austempering times (15–90 min).

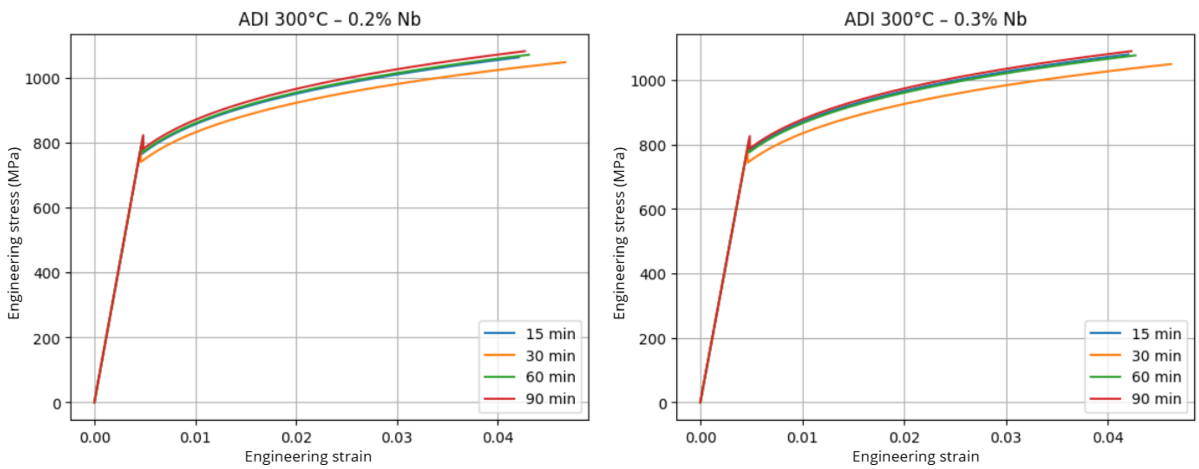

Figure 5. Engineering stress–strain curves of austempered ductile iron at 300 °C for different Nb contents (0.2 and 0.3 wt.%) and austempering times (15–90 min).

Table 2. Volume fraction (%) of high carbon austenite from 15 to 90 minutes of treatment at 250 and 300 °C with 0.2 and 0.3 % Nb.

Treatment/Alloy	ADI 0.2	ADI 0.3
Treatment/Alloy	ADI 0.2	ADI 0.3
15 min 250 °C	37.97	36.52
30 min 250 °C	38.96	41.79
60 min 250 °C	41.10	42.79
90 min 250 °C	38.38	38.07
15 min 300 °C	38.56	39.11
30 min 300 °C	41.44	42.48
60 min 300 °C	40.69	40.99
90 min 300 °C	40.00	39.21

strength and a significant increase in ductility compared to the 250 °C treatment. The effect of niobium remains as a strengthening factor through microstructural refinement and precipitation hardening; however, its influence is partially attenuated by microstructural coarsening at this temperature. The non-monotonic evolution with austempering time characterized by a decrease in strength at intermediate times followed by recovery at longer times is associated with the stabilization and subsequent partial transformation of retained austenite. Overall, these results confirm that the 300 °C treatment promotes a mechanical response suited for application where ductility and energy absorption capacity are prioritized.

Figure 6 shows the evolution of elongation for alloys containing 0.2 and 0.3 wt% Nb at 250 and 300 °C as a function of austempering time, alloying the simultaneous assessment of the effects of temperature and Nb content on the ductility of ADI. The evolution of elongation with austempering time indicates that ADI ductility is governed by the stability of retained austenite, which reaches a maximum at 30 minutes of treatment, regardless of Nb content. Conditions at 300 °C significantly enhance plastic deformation due to a higher fraction

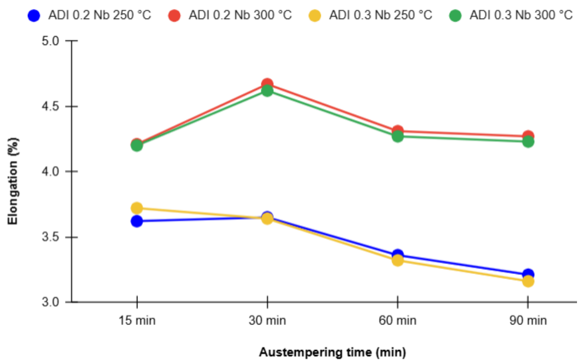

Figure 6. Elongation as a function of austempering time for different Nb contents at 250 and 300°C.

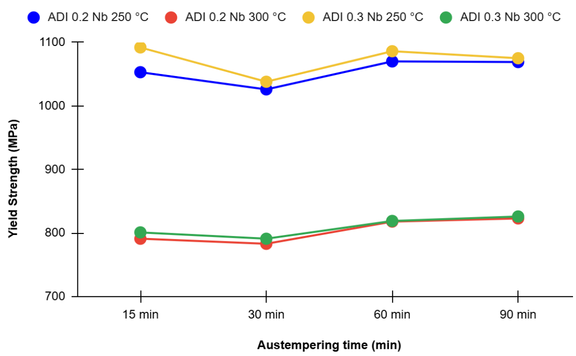

Figure 7. Yield strength (YS) as a function of austempering time for Nb-alloyed ADI at 250 and 300 °C.

and stability of this phase, promoting activation of the TRIP mechanism. In contrast, at 250 °C, the finer microstructure increases mechanical strength but limits ductility. Increasing Nb content slightly reduces elongation due to precipitation hardening and the higher carbide content; however, its effect is secondary compared to that of temperature. Overall, these results demonstrate that optimizing ductility in ADI requires precise control of austempering time 30 minutes being the optimal condition as well as appropriate selection of temperature depending on the intended application.

Figure 7 presents the variation of yield strength (YS) as a function of austempering time for ADI alloys containing 0.2 and 0.3 wt.% Nb treated at 250 and 300 °C. For both compositions, the highest YS values were obtained at 250 °C, while samples austempered at 300 °C exhibited lower values due to the formation of a coarser ausferritic microstructure and a higher retained austenite content. A minimum was observed at 30 min, which coincides with the maximum retained austenite fraction, indicating that this softer phase reduces the resistance to plastic deformation. At longer austempering times, YS gradually increased as the microstructure became more stable. Furthermore, the 0.3 wt.% Nb alloy consistently exhibited slightly higher YS values than the 0.2 wt.% Nb alloy, which may be associated with microstructural refinement and the higher NbC carbide fraction (2.48% compared to

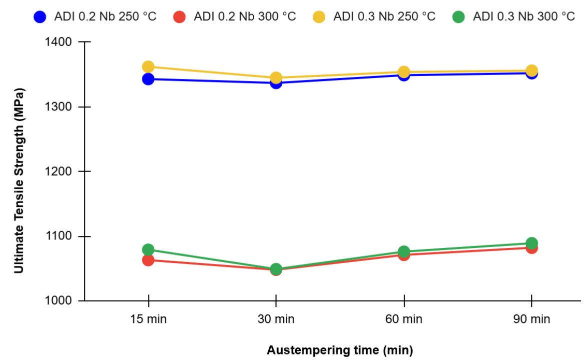

Figure 8. Ultimate tensile strength (UTS) as a function of austempering time for Nb-alloyed ADI at 250 and 300 °C.

1.51%). The differences between treatments became less pronounced at 300 °C, suggesting a reduced sensitivity of YS to niobium content at higher austempering temperatures.

The evolution of ultimate tensile strength (UTS) in ADI, shown in figure 8, demonstrates that the mechanical behavior is governed by the refinement of the ausferritic microstructure and the fraction of retained austenite. Conditions at 250 °C produce the highest UTS values due to the formation of fine ausferrite with high interfacial density, whereas at 300 °C the higher fraction of retained austenite reduces the maximum strength. The non-monotonic behavior with time characterized by a minimum at 30 minutes followed by recovery at longer times is associated with the stabilization and subsequent partial transformation of retained austenite. Nb addition consistently increases UTS through microstructural refinement and NbC precipitation hardening, being more effective at lower temperatures. Overall, these results confirm that controlling UTS in ADI requires a balance between bainitic refinement and retained austenite stability, primarily governed by the austempering temperature.

3.4 Hardness

Figure 9 shows the relationship between retained austenite volume fraction and hardness for ADI alloys containing 0.2 and 0.3 wt.% Nb austempered at 250 and 300 °C. For the 0.2 wt.% Nb alloy, hardness decreases as the retained austenite content increases, reaching a minimum value at 60 min for the 250 °C treatment (27.68 HRC) and at 30 min for the 300 °C treatment (27.68 HRC). These conditions correspond to the highest retained austenite fractions, indicating an inverse relationship between both parameters. A similar trend is observed for the 0.3 wt.% Nb alloy, where the minimum hardness values coincide with the maximum retained austenite contents. At 250 °C, the retained austenite fraction reaches 42.79% at 60 min, while hardness decreases to 29.70 HRC. Likewise, at 300 °C, the highest retained austenite

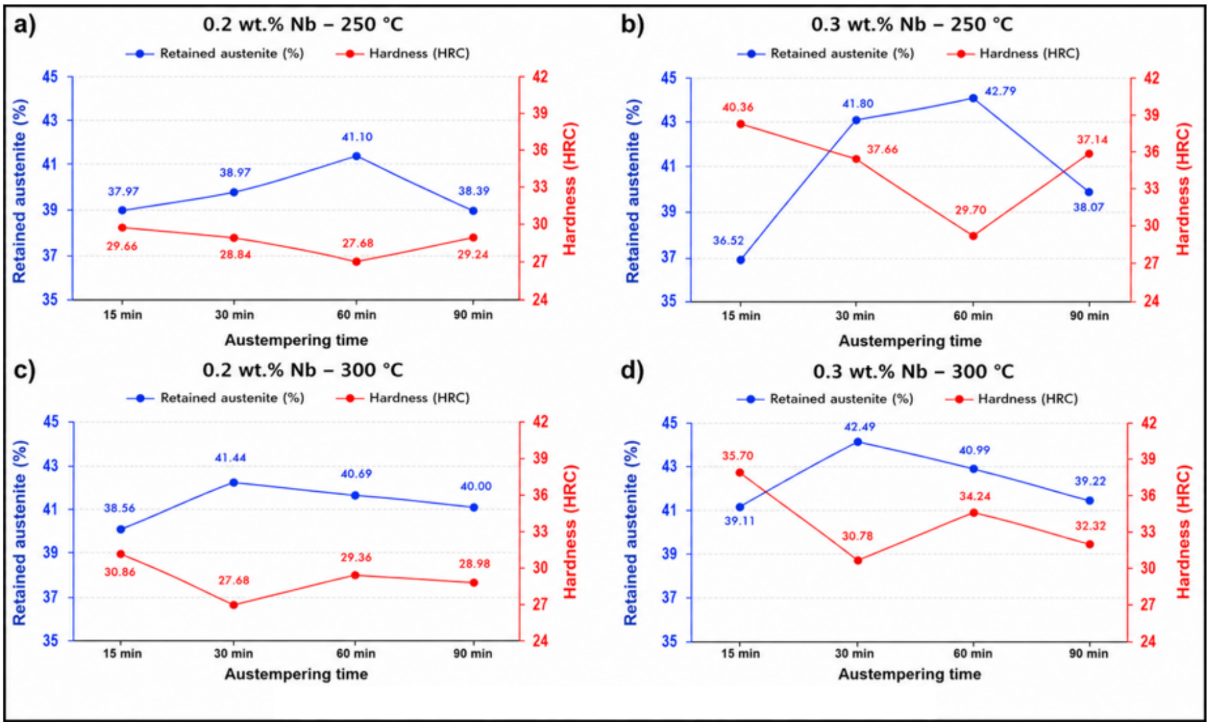

Figure 9. Evolution of retained austenite volume fraction and hardness in austempered ductile irons alloyed with 0.2 and 0.3 wt.% Nb at different austempering times. The treatments were conducted at 250 °C [(a) 0.2 wt.% Nb and (b) 0.3 wt.% Nb] and 300 °C [(c) 0.2 wt.% Nb and (d) 0.3 wt.% Nb].

content (42.49%) is observed at 30 min, corresponding to a hardness of 30.78 HRC. The reduction in hardness with increasing retained austenite content is associated with the greater proportion of high-carbon austenite, which is softer and more deformable than ferrite and carbide-containing regions. Due to its face-centered cubic (FCC) crystal structure, retained austenite facilitates dislocation motion and reduces resistance to indentation. Conversely, when the retained austenite fraction decreases, hardness tends to increase owing to the larger contribution of the ausferritic matrix and the strengthening effect associated with niobium additions. These results are consistent with previous studies reporting an inverse correlation between retained austenite content and hardness in austempered ductile irons (Cruz et al., 2022).

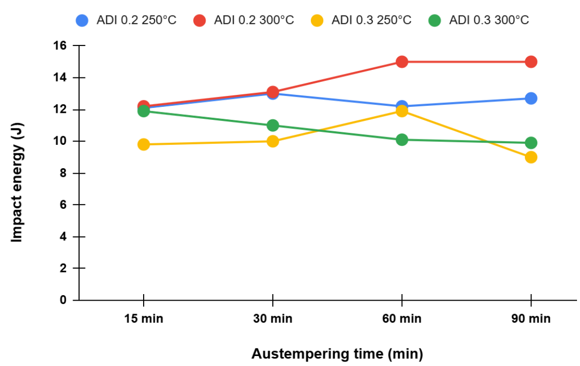

Figure 10. Charpy impact energy results, blue line is ADI 0.2, 250 °C, red line is ADI 0.2, 300 °C, yellow line is ADI 0.3 250 °C and green line is ADI 0.3, 300 °C.

3.5 *Charpy impact*

Charpy impact test results are shown in figure 10 alloys with lower niobium content exhibit better impact resistance. Impact energy is affected by both the number of carbides and the characteristics of the ausferritic matrix. Carbides act as discontinuities in the matrix and serve as crack initiation sites (Nofal *et al.*, 2002). ADIs treated at 300°C display superior impact resistance, reaching a maximum value of 15 J at 60 and 90 minutes, compared to those treated at 250 °C. This improvement is attributed to the higher volume of high carbon austenite which contributes to enhanced fracture toughness (Da Silva *et al.*, 2014). High carbon austenite improves impact resistance due its crystal structure. This ductile phase can absorb more energy by deforming plastically rather than fracturing immediately. Furthermore, an ausferritic matrix with a higher austenite content promotes more uniform stress distribution, reducing localized stress concentrations and delaying crack initiation. As a result, the material exhibits increased toughness and improved energy absorption capacity under impact condition.

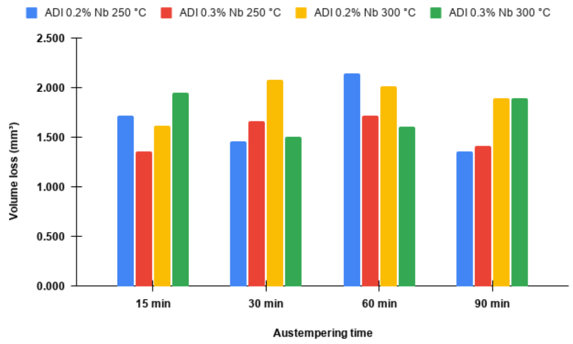

Figure 11. Wear test results, blue bar is ADI 0.2, 250 °C, red bar is ADI 0.3, 250 °C, yellow bar is ADI 0.2, 300 °C and green bar is ADI 0.3, 300 °C.

3.6 Wear test

Figure 11 shows the variation in wear volume loss of austempered ductile irons containing 0.2 and 0.3 wt.% Nb austempered at 250 and 300 °C for different holding times. In general, the wear behavior was strongly influenced by both the austempering temperature and the niobium content. At 250 °C, the alloy containing 0.3 wt.% Nb exhibited the lowest volume loss at 15 min (1.35 mm^3), indicating superior wear resistance compared with the 0.2 wt.% Nb alloy (1.72 mm^3). As the austempering time increased to 60 min, both alloys showed an increase in volume loss, reaching maximum values of 2.14 mm^3 and 1.72 mm^3 for the 0.2 wt.% and 0.3 wt.% Nb alloys, respectively. At 90 min, the wear volume decreased again, suggesting an improvement in wear resistance. For the samples austempered at 300 °C, the highest volume losses were observed at intermediate austempering times, particularly at 30 min for the 0.2 wt.% Nb alloy (2.07 mm^3). In contrast, the 0.3 wt.% Nb alloy showed lower and more stable wear losses throughout the austempering treatment, reaching a minimum value of 1.50 mm^3 at 30 min. Overall, the addition of 0.3 wt.% Nb generally improved wear resistance compared with the 0.2 wt.% Nb alloy, particularly at 250 °C. This behavior could be attributed to the strengthening effect of niobium carbides and the refinement of the ausferritic microstructure, which can increase resistance to material removal during sliding wear. Furthermore, the observed wear response may also be associated with changes in retained austenite stability and microstructural evolution induced by the austempering parameters.

Conclusions

The influence of 0.2 % and 0.3 % niobium additions on the mechanical properties of ductile iron subjected to austempering heat treatments at 250 °C and 300 °C can be summarized as follows:

1. A higher niobium content (0.3 %) promotes an increased volume of high carbon austenite, as niobium acts as a nucleation site for this phase.

2. The volume of retained high carbon austenite increases when austempering is performed at 300 °C.

3. Hardness is inversely related to the percentage of retained high carbon austenite, with higher austenite contents resulting in lower hardness values.

4. The highest Charpy impact values were recorded for the ADI 0.2 % alloy, attributed to the lower carbide content, as carbide serves as crack initiation sites and reduce impact resistance.

5. The lowest wear rates were observed in samples austempered at 250 °C, due to the reduced presence of high carbon austenite, which is a softer and more ductile phase with limited wear resistance.

6. Ductile iron with 0.3 % niobium exhibited better wear resistance than those with 0.2 % niobium, as a result of the higher carbide content. Although carbides enhance wear resistance, they also increase material brittleness.

7. The austempering temperature controls the mechanical behavior of ADI: at 250 °C, the highest YS and UTS values are obtained due to the formation of fine ausferrite, whereas at 300 °C, the higher fraction of retained austenite increases ductility through the TRIP effect.

8. Nb addition enhances mechanical strength through microstructural refinement and NbC precipitation, although it slightly reduces ductility; this effect is more pronounced at 250 °C and becomes less significant at 300 °C.

Acknowledgements

The authors would like to express their gratitude to the Secretaría de Ciencia, Humanidades, Tecnología e Innovación (SECIHTI), the Autonomous University of the State of Hidalgo (UAEH), and the National Polytechnic Institute (IPN) for their support in carrying out this project.

References

Abdullah, B., Alias, S.K., Jaffar, A., Rashid, A.A., Haskil, M. and Ramli, A. (2012). Tensile strength properties of niobium alloyed austempered ductile iron on different austempering time. *Advanced Materials Research* 457-458, 1155-1158. https://doi.org/10.4028/www.scientific.net/AMR.457-458.1155

Ahmed, M., Soliman, M., Youssef, M., Bähr, R. and Nofal, A. (2021). Effect of niobium on the microstructure and mechanical properties of alloyed ductile irons and austempered ductile irons. *Metals* 11(5), 703. https://doi.org/10.3390/met11050703

Artola, G., Gallastegi, I., Izaga, J., Barrena, M. and Rimmer, A. (2017). Austempered ductile iron (ADI) alternative material for high-performance applications. *International Journal of Metalcasting* 11(1), 131-135. https://doi.org/10.1007/s40962-016-0085-8

ASTM International (2025a). *ASTM Volume 03.01: Metals – Mechanical Testing; Elevated and Low-temperature Tests; Metallography*. ASTM Compass.

ASTM International (2025b). *ASTM Volume 03.02: Corrosion of Metals; Tribology of Solid Materials*. ASTM Compass

Avdusinovic, H. and Gigović-Gekić, A. (2009). Heat treatment of nodular cast iron. *Trends in Development of Machinery and Associated Technology*, 16-21.

Bayati, H. and Elliott, R. (1999). The concept of an austempered heat treatment processing window. *International Journal of Cast Metals Research* 11(5), 413-417. https://doi.org/10.1080/13640461.1999.11819309

Boccardo, A.D., Dardati, P.M., Godoy, L.A. and Celentano, D.J. (2018). Sensitivity of austempering heat treatment of ductile irons to changes in process parameters. *Metallurgical and Materials Transactions B* 49, 1522-1536. https://doi.org/10.1007/s11663-018-1222-y

Chen, B., Zhang, G., Wang, X., Gao, L. and Song, X. (2024). Effect of niobium content on microstructure and wear and corrosion resistance of laser-clad FeCo0.5CrNi1.5B0.5Nbx coatings on ductile iron. *Surface and Coatings Technology* 476, 130210. https://doi.org/10.1016/j.surfcoat.2023.130210

Chiniforush, E.A., Rahimi, M. and Yazdani, S. (2016). Dry sliding wear of Ni alloyed austempered ductile iron. *China Foundry* 13, 361-367. https://doi.org/10.1007/s41230-016-6072-0

Cruz, A., Colín, E., Chávez, J.F., Téllez, J. and Magaña, A. (2022). Evaluation of CADI low alloyed with chromium for camshafts application. *Metals* 12(2), 249. https://doi.org/10.3390/met12020249

da Silva, A.J.S.T., Goldenstein, H., Guesser, W.L. and de Campos, M.F. (2014). Quenching and partitioning heat treatment in ductile cast irons. *Materials Research* 17, 1115-1123. http://dx.doi.org/10.1590/1516-1439.220713

Darwish, N. and Elliott, R. (1993). Austempering of low manganese ductile irons Part 3 variation of mechanical properties with heat treatment conditions. *Materials Science and Technology* 9(10), 882-889. https://doi.org/10.1179/mst.1993.9.10.882

Dubensky, W. and Rundman, K.B. (1985). An electron microscope study of carbide formation in austempered ductile iron. *AFS Transactions* 93, 389-394.

Erfanian-Naziftoosi, H.R., Haghdadi, N. and Kiani-Rashid, A.R. (2012). The effect of isothermal heat treatment time on the microstructure and properties of 2.11% Al austempered ductile iron. *Journal of Materials Engineering and Performance* 21, 1785-1792. https://doi.org/10.1007/s11665-011-0086-y

Górny, M., Angella, G., Tyrała, E., Kawalec, M., Paź, S. and Kmita, A. (2019). Role of austenitization temperature on structure homogeneity and transformation kinetics in austempered ductile iron. *Metals and Materials International* 25, 956-965. https://doi.org/10.1007/s12540-019-00245-y

Górny, M., Gondek, L., Tyrała, E., Angella, G. and Kawalec, M. (2021). Structure homogeneity and thermal stability of austempered ductile iron. *Metallurgical and Materials Transactions A* 52, 2228-2237. https://doi.org/10.1007/s11661-021-06214-8

Janowak, J.F., Gundlach, R.B., Eldis, G.T. and Rohrting, K. (1982). Technical advances in cast iron metallurgy. *International Cast Metals Journal* 6, 28-42.

Janowak, J.F. and Norton, P.A. (1985). A guide to mechanical properties possible by austempering, 1 percent Ni, 0.3 percent Mo iron. *AFS Transactions* 88, 123-135.

Lu, G.-X. and Zhang, H. (1990). Sliding wear characteristics of austempered ductile iron with and without laser hardening. *Wear* 138(1-2), 1-12. https://doi.org/10.1016/0043-1648(90)90163-5

Mussa, A., Krakhmalev, P. and Bergström, J. (2022). Wear mechanisms and wear resistance of austempered ductile iron in reciprocal sliding contact. *Wear* 498-499, 204305. https://doi.org/10.1016/j.wear.2022.204305

Nan, R., Fu, H., Yang, P., Lin, J. and Guo, X. (2020). Microstructure evolution and wear resistance of Cu-bearing carbidic austempered ductile iron after austempering. *Journal of Materials Engineering and Performance* 29(4), 2440-2459. https://doi.org/10.1007/s11665-020-04788-9

Nofal, A.A. and Jekova, L. (2009). Novel processing techniques and applications of austempered ductile iron. *Journal of the University of Chemical Technology and Metallurgy* 44, 213-228.

Nofal, A.A., Ramadan, M. and Abdel, K.R. (2002). Effect of graphite nodularity on structure and properties of austempered cast iron. *World Conference of ADI AFS Publication* 50, 15-28

Pereloma, E.V. and Anderson, C.S. (2013). Microstructure and properties of austempered ductile iron subjected to single and two step processing. *Materials Science and Technology* 22, 1112-1118. https://doi.org/10.1179/174328406X114216

Rouns, T.N., Rundman, K.B. and Moore, D.M. (1984). The relationship between microstructure and tensile properties in ADI. *AFS Transactions* 121, 815-840.

Sckudlarek, W., Krmasha, M.N., Al-Rubaie, K.S., Preti, O., Milan, J.C.G. and da Costa, C.E. (2021). Effect of austempering temperature on microstructure and mechanical properties of ductile cast iron modified by niobium. *Journal of Materials Research and Technology* 12, 2414-2425. https://doi.org/10.1016/j.jmrt.2021.04.041

Straffelini, G., Pellizzari, M. and Maines, L. (2011). Effect of sliding speed and contact pressure on the oxidative wear of austempered ductile iron. *Wear* 270(9-10), 714-719. https://doi.org/10.1016/j.wear.2011.02.004

Swain, S.K., Panda, R.K., Mishra, J.P. and Sen, S. (2012). Phase investigation of austempered ductile iron. *Orissa Journal of Physics* 19, 73-80.

Tyrała, E., Górny, M., Kawalec, M., Muszyńska, A. and Lopez, H. (2019). Evaluation of volume fraction of austenite in austempering process of austempered ductile iron. *Metals* 9, 893. https://doi.org/10.3390/met9080893

Walton, C.F. (2018). *Gray and ductile iron castings handbook*. Society Incorporated.

Wang, B., Barber, G.C., Qiu, F., Zou, Q. and Yang, H. (2020). A review: Phase transformation and wear mechanisms of single-step and dual-step austempered ductile irons. *Journal of Materials Research and Technology* 9(1), 1054-1069. https://doi.org/10.1016/j.jmrt.2019.10.074

Wang, C., Du, X., Li, S., Sun, Y. and Yang, P. (2017). Morphology and crystallography of ausferrite in austempered ductile iron. *Metals* 7(7), 238. https://doi.org/10.3390/met7070238

Wang, H., Feng, Y., Jiang, W., Wang, C., Guo, E., Fu, Y. and Zhao, S. (2024). Effect of niobium on microstructure and mechanical properties of ductile iron with high strength and ductility. *Journal of Materials Engineering and Performance* 33, 896-905. https://doi.org/10.1007/s11665-023-08019-9

Wen, F., Zhao, J., Zheng, D. and He, K. (2019). The role of bainite in wear and friction behavior of austempered ductile iron. *Materials* 12(5), 767. https://doi.org/10.3390/ma12050767

Zhang, J., Zhang, N., Zhang, M., Lu, L., Zeng, D. and Song, Q. (2014). Microstructure and mechanical properties of austempered ductile iron with different strength grades. *Materials Letters* 119, 47-50. https://doi.org/10.1016/j.matlet.2013.12.086

Zhu, K., Barbier, D. and Iung, T. (2013). Characterization and quantification methods of complex BCC matrix microstructures in advanced high strength steels. *Journal of Materials Science* 48, 413-423. https://doi.org/10.1007/s10853-012-6756-9

Zimba, J., Simbi, D.J. and Navarra, E. (2003). Austempered ductile iron: An alternative material for earth moving components. *Cement and Concrete Composites* 25(6), 643-649. https://doi.org/10.1016/S0958-9465(02)00078-1